frontiers in Environmental Chemistry

ORIGINAL RESEARCH
published: 29 October 2020
doi: 10.3389/fenvc.2020.599349

Insight Into the Role of Ceria on OMS-2 and OL Materials for Catalytic Degradation of Toluene

*Lin Yue[1,2], Minghua Hu[1], Mingjiao Tian[2], Xu Liao[3], Zhihua Xu[1], Ling Shi[1] and Chi He[2]**

[1]Hubei Key Laboratory of Industrial Fume and Dust Pollution Control, Jianghan University, Wuhan, Hubei, China, [2]State Key Laboratory of Multiphase Flow in Power Engineering, School of Energy and Power Engineering, Xi'an Jiaotong University, Xi'an, Shaanxi, China, [3]Key Laboratory of Urban Environment and Health, Institute of Urban Environment, Chinese Academy of Sciences, Xiamen, China*

Catalytic oxidation is one of the most efficient approaches for industrial volatile organic compounds (VOCs) elimination. MnO_x-based catalysts have attracted much attention due to their remarkable low-temperature catalytic activity. Here, octahedral layered birnessite-type manganese oxide (OL-1) with layer spacing of 7 Å and cryptomelane type manganese oxide (OMS-2) with tunneled pore diameter of 4.6 Å× 4.6 Å were synthesized by a reflux method. Following this, Ce-doped OL-1 and OMS-2 were further prepared by an impregnation method with target to improve catalytic performance in toluene oxidation. Results reveal that the OMS-2 material exhibits the best catalytic activity with 90% of toluene decomposed at 224°C owing to the presence of a large quantity of active lattice oxygen species. Interestingly, the introduction of Ce leads to the formation of large amounts of acidic sites, which limit the oxidation process and enhance the yield of benzoic acid by-product. The findings in the present work are meaningful for deepening our understanding of the role of ceria on metal oxide catalysts and helping us to design effective catalysts for VOC destruction.

Keywords: Volatile organic compounds, Ce/MnO_x, toluene, catalytic oxidation, reaction mechanism

OPEN ACCESS

Edited by:
Dengsong Zhang,
Shanghai University, China

Reviewed by:
Xiaodong Zhang,
University of Shanghai for Science and Technology, China
Xiaolin Yu,
Institute of Chemistry (CAS), China

****Corresponding author:***
Chi He
chi_he@xjtu.edu.cn

Specialty section:
This article was submitted to Catalytic Remediation, a section of the journal Frontiers in Environmental Chemistry

Received: *27 August 2020*
Accepted: *22 September 2020*
Published: *29 October 2020*

Citation:
Yue L, Hu M, Tian M, Liao X, Xu Z, Shi L and He C (2020) Insight Into the Role of Ceria on OMS-2 and OL Materials for Catalytic Degradation of Toluene. Front. Environ. Chem. 1:599349. doi: 10.3389/fenvc.2020.599349

INTRODUCTION

Volatile organic compounds (VOCs) are one of the major contributors to the formation of secondary pollutants (e.g., tropospheric ozone, PAN, and secondary organic aerosols) and photochemical smog, leading to a large decline in air quality and consequently concerns regarding human health (Menon et al., 2011; Wu et al., 2016; He et al., 2019). Nowadays, rapid urbanization and industrialization contribute to rapidly increasing VOCs emissions, and the reduction and control of VOCs from anthropogenic sources is becoming a research hotspot in the world. Among a variety of technologies (e.g., adsorption, absorption, condensation, and combustion), catalytic oxidation which completely decompose VOC molecules into harmless carbon dioxide and water under mild reaction conditions is regarded as one of the most effective and economically feasible strategies for industrial VOC removal (Wu et al., 2016).

Manganese oxides as one type of powerful catalysts for VOC oxidation have attracted much attention recently (Shen et al., 1996; Luo et al., 2000; Tian et al., 2011; Iyer et al., 2012). Among them, two-dimensional (2D) layered birnessite-type manganese oxide (OL-1; layer spacing of

7 Å) with exchangeable metal cations (e.g., K^+ and Na^+) and porous octahedral layered birnessite-type manganese oxide (OMS-2; pore diameter of 4.6 Å × 4.6 Å) exhibit great advantages in VOC catalytic elimination due to their porous structure, mixed valence of Mn and abundant lattice oxygen (Luo et al., 2000; Nyutu et al., 2008; Tian et al., 2011; Hou et al., 2014; Luo et al., 2015). Sun et al. (2011) proposed that the refluxing method is better than solid-reaction method for the preparation of OMS-2 material with superior catalytic performance in toluene oxidation. In general, more lattice oxygen and high oxygen mobility of OMS-2 materials were thought to be the main factors for their superior catalytic activity. It is well known that the amounts of lattice oxygen and oxygen mobility of a catalyst are closely related to material morphology and structure and doped metal ions (Jiang et al., 2018; Yan et al., 2019). Cerium oxide has attracted much attention in catalysts and been used as a promoter for enhancing the catalytic activity due to its high oxygen-storage capacity (OSC) and facile redox cycle of Ce^{4+}/Ce^{3+} (Luo et al., 1998; Zhou et al., 2009; Arena et al., 2015). For instance, hierarchical layer-stacking Mn-Ce composite oxides were investigated for catalytic combustion of benzene, toluene and ethyl acetate (Tang et al., 2015), and found that the introduction of Ce increased the amounts of active surface oxygen over prepared materials and subsequently possessing higher catalytic activity. Chen X. et al. (2018) reported that mesoporous CeO_2 (CeO_2-MOF) possesses higher activity in catalytic destruction of toluene than that of CeO_2 prepared by precipitation method due to its larger specific surface area, smaller average grain size, higher oxygen storage capacity, higher surface oxygen and higher relative percentage of Ce^{3+}/Ce^{4+}.

In recent years, Ce/OMS-2 material has been used for CO oxidation (Santos et al., 2014), dimethyl ethyl oxidation (Yu et al., 2011), formaldehyde oxidation (Wang and Li, 2009), aroused concerns of researchers. Ce ions not only can incorporate into OMS-2 tunnel to substitute K^+, but also can incorporate into OMS-2 framework to substitute Mn ion, which cause the structure change (Wang and Li, 2009; Yu et al., 2011; Santos et al., 2014). Up to now, the effects of the addition of Ce on manganese oxides molecular sieves with different morphologies and structures are obscure. In this work, two types of manganese oxides (OL-1 and OMS-2) with different morphologies and structures were prepared and adopted as supports for ceria. All synthesized materials were extensively characterized by different technologies including X-ray diffraction (XRD), low-temperature N_2 sorption, scanning electron microscope (SEM), transmission electron microscopy (TEM) and high-resolution TEM, X-ray fluorescence, temperature programmed reduction of H_2 (H_2-TPR), temperature programmed desorption of NH_3 (NH_3-TPD), X-ray photoelectron spectroscopy (XPS) and *in situ* diffuse reflectance Fourier transform infrared spectroscopy (*in situ* DRIFTS). Toluene as a common VOC was selected as the probe pollutant to evaluate the catalytic performance of synthesized catalysts. In addition, the catalytic mechanisms of toluene oxidation over Ce-doped catalysts were further proposed.

EXPERIMENTAL

Catalyst Preparation

OMS-2 material was synthesized *via* the reaction between MnO_4^- and Mn^{2+} through a reflux method (Kingondu et al., 2011). A solution consisted of $MnSO_4{\cdot}H_2O$ (4.4 g, 26.0 mmol), concentrated HNO_3 (1.5 ml), and deionized water (15.0 ml) was stirred for 30 min (solution A). The second solution (solution B) was prepared by dissolving 38 mmol of $KMnO_4$ in 100 ml of deionized water. Then the solution B was subsequently added into solution A under vigorous stirring at 100°C for 24 h until the color of the solution turned to a dark brown. Finally, the obtained product was washed with deionized water, filtered, and dried at 110°C overnight to gain the OMS-2 sample (denoted as OMS).

OL-1 material containing potassium was synthesized according to a method reported by Iyer et al. (2012). A solution containing 92 ml of ethanol and 33.6 g of potassium hydroxide was firstly prepared. The other solution dissolving 9.48 g of potassium permanganate in 150 ml of deionized water was prepared, and the former solution was slowly added into the latter solution under vigorous stirring. The mixture was stirred for 1 h and aged at 80°C for 48 h. The resulting product was washed with deionized water until the pH value lower than 9.0, and then dried at 80°C overnight to obtain the OL-1 sample named OL.

Ce-doped catalysts were prepared by an impregnation method. Typically, 1.67 g of cerium nitrate hydrate ($Ce(NO_3)_3{\cdot}6H_2O$) was dissolved in 25 ml of H_2O and mixed with 5 g of prepared OMS-2 or OL-1, and then evaporated at 60°C for 4 h. After this, the obtained samples were dried at 120°C for 8 h. All resulting samples mentioned above were calcined at 400°C for 4 h with a heating rate of 10°C/min, and referred to as CeOMS and CeOL, respectively.

Catalyst Characterizations

XRD were performed on a powder diffraction system (X'Pert PRO; PANalytical, Almelo, The Netherlands) equipped with Cu Kα radiation (λ = 0.15418 nm) in 2θ range of 5°–80° (scanning rate of 3°/min). N_2 adsorption/desorption isotherms of catalysts were collected at 77 K on a gas sorption analyzer ASAP 2020M. All samples were pretreated at 350°C under vacuum for 4 h before measurement. The total pore volume and specific surface area (S_{BET}) were estimated from the amount of nitrogen adsorbed at a relative pressure (P/P_0) of 0.05–0.30, and the value of S_{BET} was calculated using the Brunauer-Emmett-Teller method. The morphology and microstructures of samples were characterized by a Hitachi su8010 scanning electron microscope operating at 15 kV. TEM and high-resolution TEM images of prepared catalysts were performed by a Talos F200S (Thermos Fisher) electronic microscopy. The elemental compositions of prepared samples were analyzed by X-ray fluorescence in a ZSX-Primus II spectrometer with Rh tube as excitation source. XPS (ESCALAB 250Xi instrument; ThermoFisher Scientific, United States) was undertaken using monochromatic Al Kα radiation, and the curve fitting was performed with the CasaXPS software.

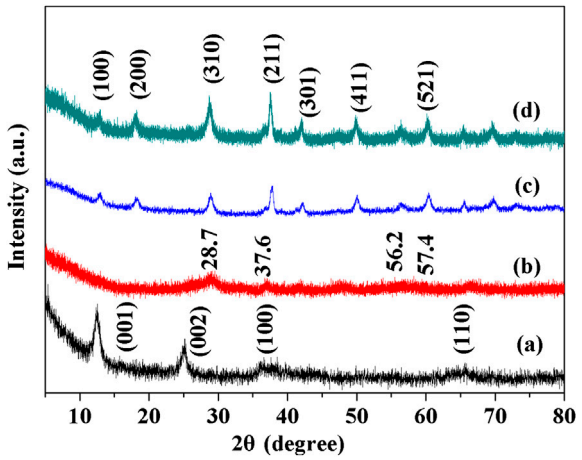

FIGURE 1 | XRD patterns of prepared catalysts: **(A)** OL, **(B)** CeOL, **(C)** OMS, and **(D)** CeOMS.

Temperature programmed reduction of H_2 (H_2-TPR) was performed on a Finetec Finesorb-3010. H_2-TPR profiles were acquired by passing 10 vol.% H_2/He flow (15 ml/min) through the catalysts (about 20 mg) which had been pre-treated in a helium flow (15 ml/min) at 300°C for 1 h. Catalyst acidity was evaluated by temperature programmed desorption of NH_3 (NH_3-TPD) on the same apparatus used with H_2-TPR. Typically, 0.1 g of the catalyst was pre-treated in a pure helium flow (30 ml/min) at 300 °C for 1 h and then cooled to room temperature prior to adsorption of NH_3 (0.5 vol% NH_3/He). After being saturated with NH_3, the catalyst was flushed with pure helium flow (30 ml/min) for 1 h at room temperature to remove the physisorbed NH_3 from the catalyst surface. Finally, the desorption profiles were recorded from 25 to 800°C with a heating rate of 10°C/min.

In situ DRIFTS of toluene oxidation was performed on a Bruker Vertex 70 (Bruker, Germany) infrared spectrometer, and all spectra were performed at a resolution of 4 cm^{-1} with 100 scans. KBr window was fitted on a reaction cell (Harrick Scientific) which connected to a purging and adsorption gas control system. After the samples were pre-treated under N_2 at 350°C for 1 h, the background was taken at every selected temperature in high-purity N_2 gas. And then, the samples with a flow of a gas mixture containing 1,000 ppm of toluene and 20 vol.% O_2/N_2 were characterized at selected temperatures.

Catalytic Activity

All evaluation experiments were performed on a fixed-bed reactor of steel tube (6 mm, i.d.) at atmospheric pressure. In each test, 0.1 g of catalyst (40–60 mesh) was placed into the tube reactor. The toluene-containing gas was generated by bubbling air through a VOC saturator, and then further diluted with another air stream (Tian et al., 2018). The total flow rate was held at 150 ml/min, i.e., gas hourly space velocity of 30,000 h^{-1} with toluene concentration of 1,000 ppm. The reaction temperature increased to a designed temperature point and kept this temperature for 30 min before each test began. Online analysis was carried out on GC (Trustworthy Instrument GC-7806) equipped with FID detector.

RESULTS AND DISCUSSION

Structure and Morphology

The XRD patterns of OMS, OL, CeOMS and CeOL catalysts are shown in **Figure 1**. All peaks of OMS material can be assigned to the pure cryptomelane phase (JCPDS #29-1020). The synthesized CeOMS sample has similar XRD patterns without any other metal oxide diffraction peak. It indicates a highly dispersed of Ce are formed or Ce crystallites are too small to be detected (Wang and Li, 2009). Meanwhile, the broader and obvious diffraction peaks of Ce-containing materials reflect the high crystallinity and small particle size of prepared material. As reported, a smaller size of cerium ions is easier to enter the tunnel microstructures of OMS-2 to exchange potassium cations (Zhang et al., 2016). This indicates that Ce ions may be incorporated into cryptomelane structure of OMS-2 material (Liu et al., 2010). XRD pattern of OL conforms to the pure K^+-birnessite phase, while the OL material has lower and broader diffraction peaks, indicating a lower crystallinity of OL catalyst. The peaks at 28.7°, 37.6°, 56.2°, and 57.4° appeared over CeOL sample suggest the presence of MnO_2 phase (JCPDS #50-0866) and no cerium oxides can be observed (Zhang et al., 2015). The diffraction peaks with the addition of Ce are turning rough and translocated, meaning that Ce-containing OL material has a lower crystallinity.

Figure 2 shows the SEM and HR-TEM images of prepared materials. OMS-2 and CeOMS samples display a typical uniform nanofiber-like morphology with 20–30 and 500 nm in diameter and length, respectively (**Figures 2C,D**). Both of the OL and CeOL materials show a nanosheet-like morphology (**Figures 2A,B**). The introduction of Ce leads to a slight aggregation of OMS and OL nanostructures. The lattice fringe spacing of OL and OMS materials in **Figures 2E,G** is 0.49 nm, which is attributed to the (200) D-space of MnO_2. As shown in **Figure 2F**, the lattice fringes of CeOL material at 0.69 nm correspond to the (110) plane of MnO_2. Compared with OMS material, the lattice fringe spacing of CeOMS material decreases to 0.31 nm, and the corresponding lattice plane becomes the (310) plane of MnO_2 (**Figure 2H**). It reveals that the introduction of Ce change crystal phase of prepared materials.

The specific surface area (S_{BET}) and total pore volume (D_v) of prepared materials are presented in **Table 1**. The specific surface areas of prepared materials decrease as follows: CeOMS (72.1 m^2/g) > CeOL (71.1 m^2/g) > OMS (67.0 m^2/g) > OL (23.4 m^2/g). Compared to OMS (0.8 cm^3/g) and OL (0.6 cm^3/g) samples, the total pore volume of Ce-doped samples (1.6 cm^3/g for CeOMS and 1.8 cm^3/g for CeOL) increases remarkably. The higher S_{BET} and larger D_v of Ce-doped samples attribute to the stacking-type pores of CeO_2 nanoparticles (Chen J. et al., 2018), in consistent with SEM results (**Figure 2**). The Ce loadings of the catalysts are listed in **Table 2**. The contents of Ce are 7.0 wt.% for CeOMS and 10.7 wt.% for CeOL.

Acidity

NH_3-TPD was used to evaluate the acid strength and acidity of prepared materials, as displayed in **Figure 3**. Only two NH_3

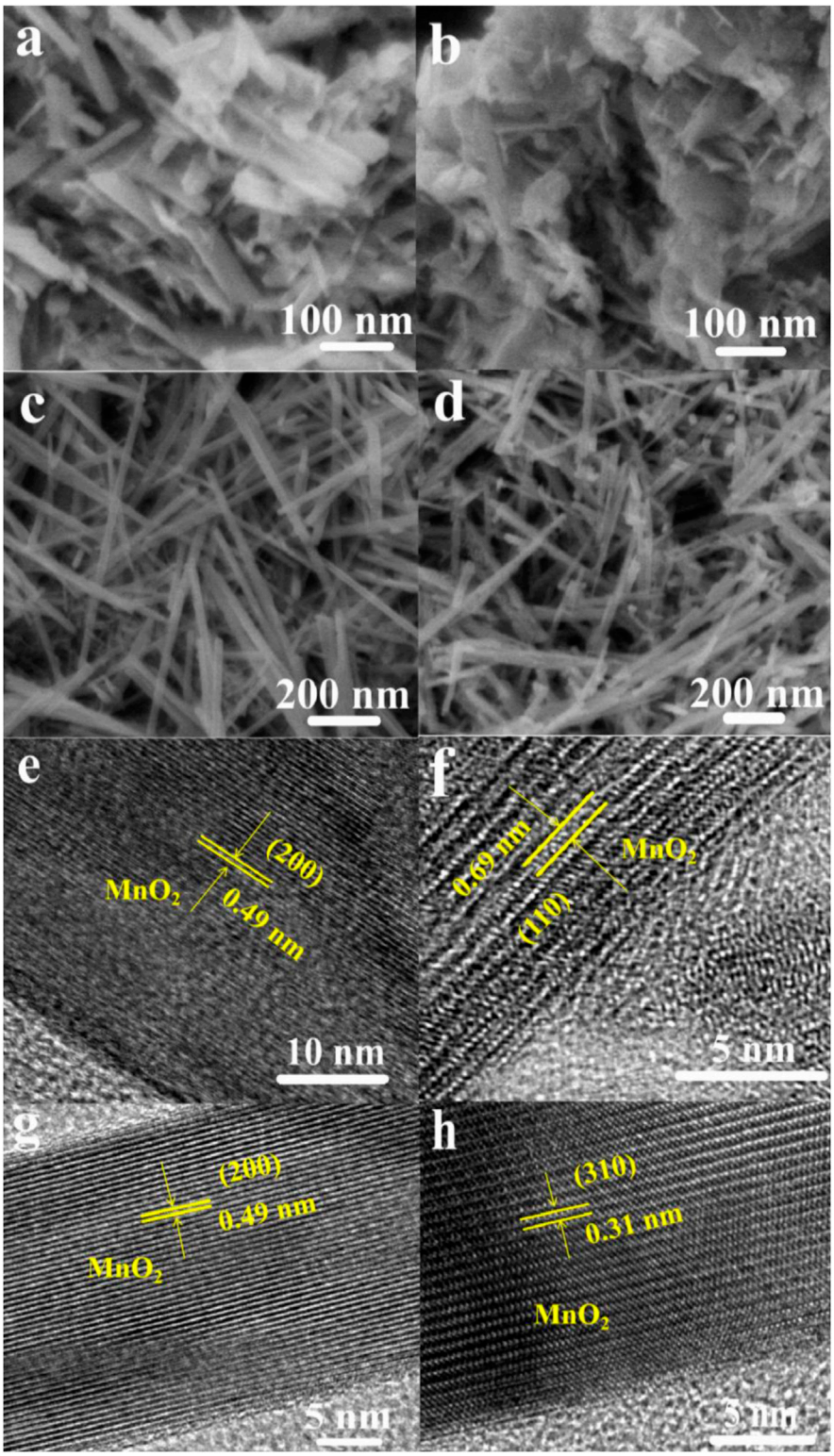

FIGURE 2 | SEM images of prepared catalysts: **(A)** OL, **(B)** CeOL, **(C)** OMS, and **(D)** CeOMS; HR-TEM images of **(E)** OL, **(F)** CeOL, **(G)** OMS, and **(H)** CeOMS.

TABLE 1 | Physicochemical properties and catalytic activity of synthesized catalysts.

Sample	S_{BET}[a] (m^2/g)	D_v[b] (cm^3/g)	Ce[c] (wt%)	T_{50}[d] (°C)	T_{90}[d] (°C)
OMS	67.0	0.8	—	216	224
CeOMS	72.1	1.6	7.0	222	230
OL	23.4	0.6	—	244	289
CeOL	71.1	1.8	10.7	272	319

[a]*Specific surface area obtained at* P/P_0 *= 0.05–0.30.*
[b]*Total pore volume estimated at* P/P_0 *= 0.99.*
[c]*Ce content analyzed by XRF.*
[d]*Temperatures at which 50% and 90% conversion of toluene.*

TABLE 2 | Surface elemental composition and status of prepared catalysts.

Catalyst	Element content (%)			Ce^{3+}/Ce^{4+}	Mn^{3+}/Mn^{4+}	$O_I/(O_I+O_{II})$[a]
	Mn	Ce	O			
OL	27.5	—	61.2	—	0.9	0.81
CeOL	25.6	4.2	65.9	0.5	1.0	0.77
OMS	29.6	—	55.8	—	0.6	0.85
CeOMS	28.3	3.6	56.0	0.4	1.1	0.84

[a]*The ratio of lattice oxygen* (O_I) *and total oxygen species* (O_I+O_{II}).

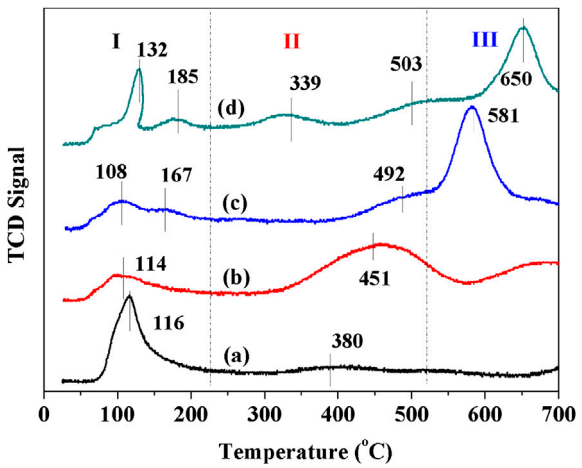

FIGURE 3 | NH_3-TPD profiles of prepared catalysts: **(A)** OL, **(B)** CeOL, **(C)** OMS, and **(D)** CeOMS.

desorption peaks can be observed over OL and CeOL catalysts (**Figure 3A**). The peak at around 110°C attributes to the weak acid sites (He et al., 2010), and the desorption peak in 200–500°C corresponds to the strong acid sites, which play a key role in catalytic reactions (He et al., 2010). CeOMS catalyst has the strongest acidity as desorption occurs at highest temperature point at each temperature zone (185°C in low-temperature zone, 503°C in medium-temperature zone, and 650°C in relative high-temperature zone). The NH_3 desorption amount was further calculated from the peak area over NH_3-TPD profiles, as given in **Table 3**. It is shown that the amounts of total acid sites over prepared materials follow the order of CeOMS > OMS > CeOL > OL. In addition, the introduction of Ce increases the amount of strong acid sites over OL and OMS catalysts with the order of CeOMS > CeOL > OMS > OL.

TABLE 3 | Acid property of prepared catalysts.

Sample	Desorption temperature (°C)			Peak area			
	I	II	III	I	II	III	Total
OL	116	380	—	343.2	160.8	—	504.0
CeOL	114	451	—	0.8	772.0	—	772.8
OMS	108,167	492	581	302	422.2	448.4	1,172.6
CeOMS	132,185	339,503	650	305	903	723	1,931

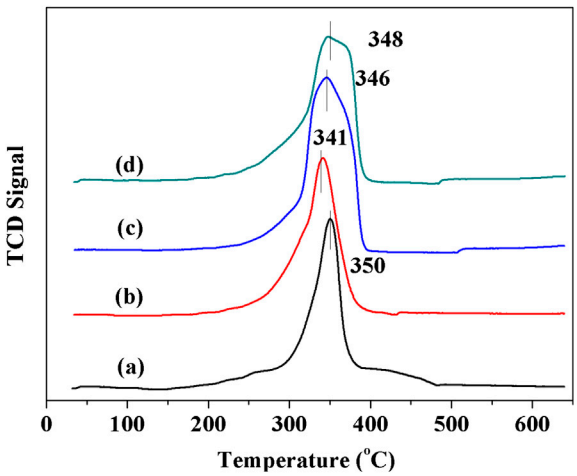

FIGURE 4 | H_2-TPR profiles of prepared catalysts: **(A)** OL, **(B)** CeOL, **(C)** OMS, and **(D)** CeOMS.

Reducibility

The reducibility of synthesized materials was characterized by H_2-TPR, as displayed in **Figure 4**. All catalysts show overlapped reduction peaks in temperature range of 330–360°C. For OMS-2 sample, the peak in 330–360°C can be attributed to the reduction of MnO_2/Mn_2O_3 to Mn_3O_4 and Mn_3O_4 to MnO (Sun et al., 2011). There is no significant difference between the temperature of reduction peaks for OMS and CeOMS. Compared to OL, the reduction peak of CeOL shifts to a lower temperature, suggesting that the reducibility of OL is promoted by introduction of cerium oxides. The hydrogen consumption calculated by the area of reduction peaks indicates the mobility of oxygen species in catalysts (Jiang et al., 2018). The H_2 consumptions over CeOL, OL, CeOMS and OMS catalysts are 11.2, 11.3, 12.4 and 13.6 mmol/g, respectively. According to the results of H_2 consumption, the reducibility of materials follows the order of OMS > CeOMS > OL > CeOL. There is no significant reduction peak of cerium oxides in the profiles of Ce-containing materials.

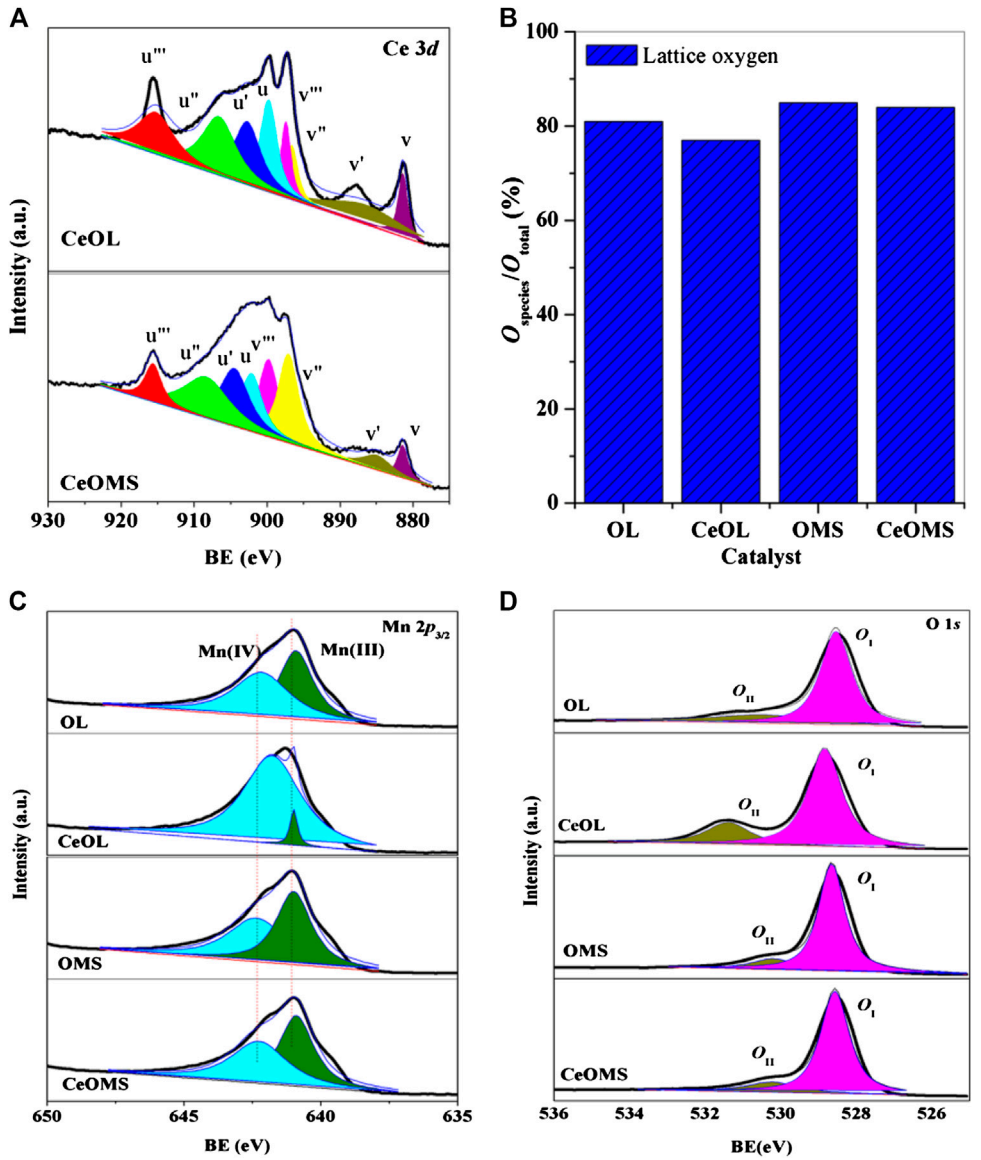

FIGURE 5 | (A) Ce 3*d*, **(C)** Mn 2*p*, **(D)** O 1*s* XPS, and **(B)** the relative ratio of lattice oxygen species determined by O 1*s* XPS spectra of prepared catalysts.

Surface Element Composition and Status

XPS was used to determine the surface element composition and chemical status of prepared catalysts. The high-resolution XPS spectra of Mn 2*p*, Ce 3*d*, and O 1*s* core levels are shown in **Figure 5**, and the surface compositions of prepared materials are listed in **Table 2**. As presented in **Figure 5A**., Ce 3*d* XPS curves could be fitted into eight peaks corresponding to two spin-orbit components (U and V) to distinguish Ce^{3+} and Ce^{4+} (Chen et al., 2011). Six features (u, u", u"', v, v", and v"') refer to the spectrum of Ce^{4+}, while the other two features (u' and v') refer to the spectra of Ce^{3+}. As shown in **Table 2**, the surface atom percentage of Ce over CeOL (4.2%) is higher than that of CeOMS (3.6%) and the values of Ce^{3+}/Ce^{4+} over CeOL and CeOMS catalysts are 0.5 and 0.4, respectively.

Mn 2*p* spectra of all catalysts are decomposed into two peaks (**Figure 5C**). Mn^{3+} (640.9 eV) and Mn^{4+} (642.2–642.4 eV) can be observed in XPS spectra (Hou et al., 2014), and the ratios of Mn^{3+}/Mn^{4+} over prepared materials are displayed in **Table 2**. With the introduction of Ce, the amounts of Mn^{4+} decrease. The values of Mn^{3+}/Mn^{4+} follow the order of OMS (0.6) < OL (0.9) < CeOL (1.0) < CeOMS (1.1). A plausible explanation for this phenomenon is an interaction effects between Ce and Mn ions, as follows:

$$Ce^{3+} + Mn^{4+} \rightarrow Mn^{3+} + Ce^{4+} \quad (1)$$

The XPS spectra of O 1*s* core electron levels for prepared catalysts are displayed in **Figure 5D**. The O 1*s* spectra can be arranged into two main regions: the lattice oxygen (O_I) in 528.5–528.8 eV and

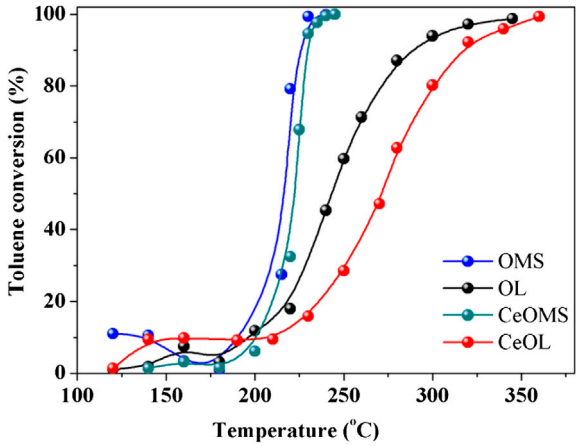

FIGURE 6 | Catalytic activity of synthesized materials for toluene decomposition.

the surface oxygen species (O_{II}) in 530.1–530.4 eV (Zhang et al., 2016). The amounts of O_I and O_{II} species are shown in **Table 2** and **Figure 5B**. The value of $O_I/(O_I+O_{II})$ is 0.81, 0.77, 0.85, and 0.84 for OL, CeOL, OMS, and CeOMS, respectively. The CeOL catalyst has the lowest lattice oxygen concentration among these samples, and OMS and CeOMS materials have similar amounts of lattice oxygen on their surface.

Catalytic Activity

The toluene conversion over prepared catalysts is presented in **Figure 6**. **Table 3** lists the reaction temperatures at which 50% (T_{50}) and 90% (T_{90}) toluene are converted. According to T_{50}, the activity sequence of catalysts is: OMS (216°C) > CeOMS (222°C) > OL (244°C) > CeOL (272°C). OMS exhibits the highest catalytic activity for toluene oxidation and achieves 90% of toluene converted at 224°C. Noticeably, the introduction of Ce not improves the catalytic performance of OMS material, and CeOL even shows a lower activity than that of OL catalyst.

Figure 7 reveals the factors (S_{BET}, the amounts of acidic sites, H_2 consumption and the ratio of lattice oxygen) corresponding to the catalytic activity of prepared materials. In **Figure 7A**, the specific surface area of OMS catalysts not relate to the catalytic activity. It is well known that toluene diameter is *ca.* 6.5 Å, while OMS-2 has the tunnel dimension of 4.6 Å × 4.6 Å (Luo et al., 2015), indicating that the catalytic reaction occurs on the external surface of OMS-2. The thickness of OL-1 layers is 7 Å, and the toluene molecules are easier to enter the interspace of OL structure. Consequently, there are more opportunity to participate in adsorption and catalytic reaction. However, the catalytic performance of toluene oxidation over OL catalyst is not as good as that of OMS. The order of lattice oxygen content displayed in **Figure 7B** over OL, OMS, CeOMS and CeOL catalysts increases as follows: CeOL < OL < CeOMS < OMS, in well agreement with the activity order. It is believed that the amount of lattice oxygen is a main factor determining the catalytic performance. Meanwhile, the H_2 consumption results in **Figure 7A** reveal that the area of H_2 reduction peak is attributing to the amounts of active oxygen species, and the reduction area order is consistent with that of the catalytic performance. This indicates the vital role of the active oxygen species in the catalytic oxidation of toluene over these catalysts. It can be speculated Ce ions occupy a certain amount of active sites and block the toluene oxidation process over manganese oxides. Catalytic oxidation of VOCs over different manganese oxides were reported to proceed by the Mars-van Krevelen mechanism (Li et al., 2010; Sun et al., 2013). As such, the catalytic oxidation of toluene in this work processes as: toluene molecules adsorbed on the surface of catalysts are oxidized by lattice oxygen species and the resultant oxygen vacancies become a crucial index during the reaction. After this, the oxygen vacancies could be replenished by oxygen in the air stream. As shown in **Figure 8**, OMS with more amounts of lattice oxygen species affords a swift redox cycling. In addition, the crystal phase of the prepared materials has not obvious effects on the catalytic performance of during toluene oxidation. The amounts of strong acid sites increase with the introduction of Ce in OL and OMS catalysts. Wang and Li (2010) proposed that a strong adsorption of reactants or products on the acid sites can block the active center and prolong the reaction process. Similarly, OMS-2 with a large quantity of weak acid sites has superior higher catalytic activity than that of CeOL and

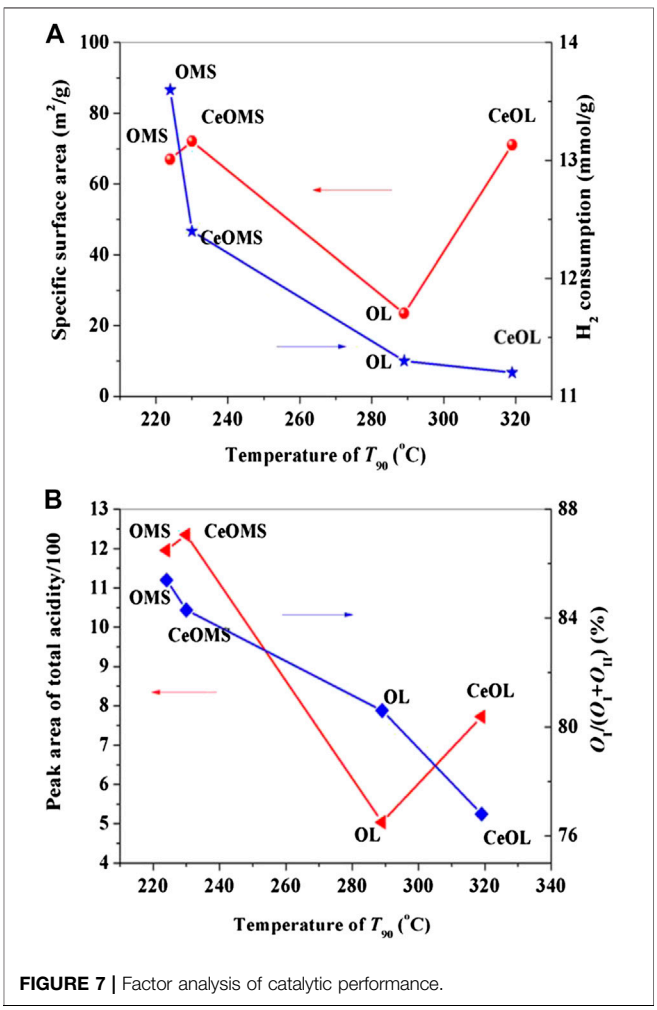

FIGURE 7 | Factor analysis of catalytic performance.

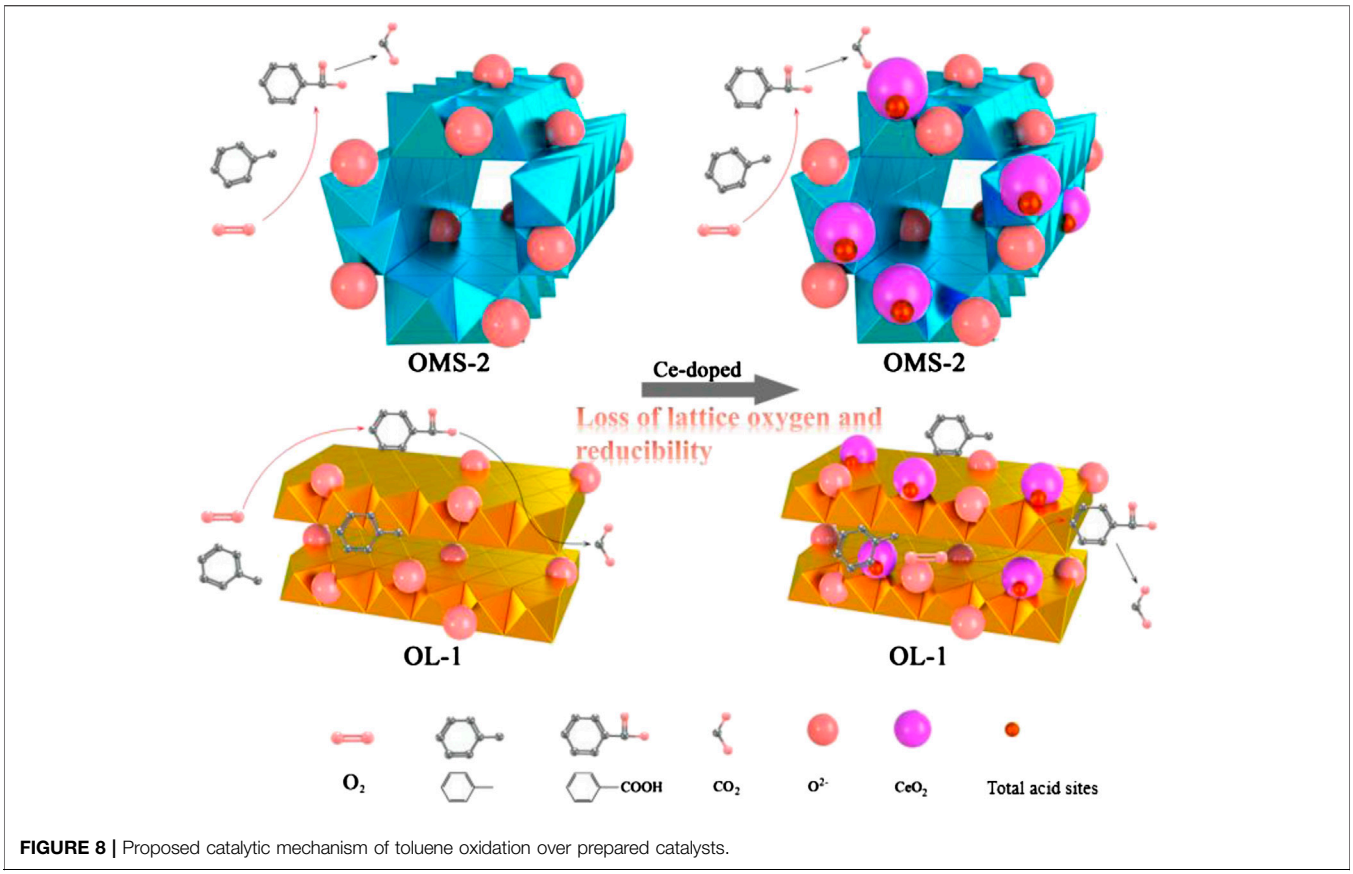

FIGURE 8 | Proposed catalytic mechanism of toluene oxidation over prepared catalysts.

CeOMS. Therefore, the catalyst with more lattice oxygen and weaker acidity possesses a better catalytic performance.

Reaction Mechanism

In situ DRIFTS experiments showed in **Figure 9** were used to investigate the catalytic reaction mechanism of toluene oxidation over synthesized catalysts. A strong peak at 3,274 cm^{-1} assigns to hydrogen-bonded OH stretching vibrations (Wu et al., 2014; Pan et al., 2017), which becomes broader and stronger with increasing of temperature from 130 to 200°C as the enhancing of reaction temperature promotes the consumption of toluene and consequently releases blank Brønsted acid. The band at 3,040 cm^{-1} corresponds to $\nu_{C\text{-}H}$ of aromatic ring (**Figure 9A**) (Li et al., 2011). A weak band at 2,321 cm^{-1} indicates a production of CO_2 (Qu et al., 2013). The bands at 1,547, 1,428, and 1,382 cm^{-1} associate with the formation of carboxylate group (-COOH) (Wang et al., 2018), and bands at 1,260 cm^{-1} correlate to C-O stretching vibration (Zhu et al., 2015). It confirms that benzoic acid is a by-product in toluene oxidation over OL catalysts (**Figure 8**).

In **Figure 9B**, the bands at 3,274, 3,040, and 2,321 cm^{-1} also display on OMS catalyst. The peaks at 2,878, 2,930, 3,040, and 3,072 cm^{-1} are attributed to the C-H stretching vibration bands of the aromatic rings and C-H symmetric or asymmetric stretching of methylene (-CH_2) (Wang et al., 2018). Besides, peaks at 1,611, 1,506, and 1,444 cm^{-1} correspond to the characteristic bands of aromatic rings (ν(C=C)) (Monney et al., 1998). A weak peak at 1,391 cm^{-1} is characteristic of typical carboxylate group (Chen X. et al., 2018). As shown in **Figure 9C**, the characteristic bands locate at the same position as the peaks of OMS in the range of 2,000–4,000 cm^{-1}. Bands at 1,260, 1,428, and 1,547 cm^{-1} can be also observed in **Figure 9A**. The IR bands of CeOMS catalyst are presented in **Figure 9D**. Prominent peaks appear at 3,274, 1,547, and 1,428 cm^{-1}, and no obvious toluene characteristic peak can be observed. Weak signals observed at 2,321 and 1,391 cm^{-1} are due to the CO_2 and carboxylate group. In these catalysts, benzoic acid is the only intermediate that can be detected in toluene oxidation, and the intensity of the bands representing carboxylate group increases with the raising of temperature. **Figure 8** elucidates that toluene oxidizes to CO_2 on prepared catalysts *via* a process of toluene oxidation to benzoic acid. As shown in **Figure 9**, the intensity of band representing carboxylate group (1,391 cm^{-1}) on OMS catalyst is weaker, indicating that less intermediates form on OMS catalyst in catalytic oxidation of toluene. The reasons can be as follows: firstly, the formation of benzoic acid is limited by the pore of OMS-2. Secondly, faster reaction processes over OMS catalyst reduce the amounts of by-products. It is reported that larger amounts of by-products form during the catalytic processes of methyl-ethyl-ketone combustion with the increments of strong acid sites (Arzamendi et al., 2009). As such, the introduction of Ce with more acid sites also increases the amounts of benzoic acid forming in catalytic oxidation of toluene as shown in the results of *in situ* DRIFTS experiments.

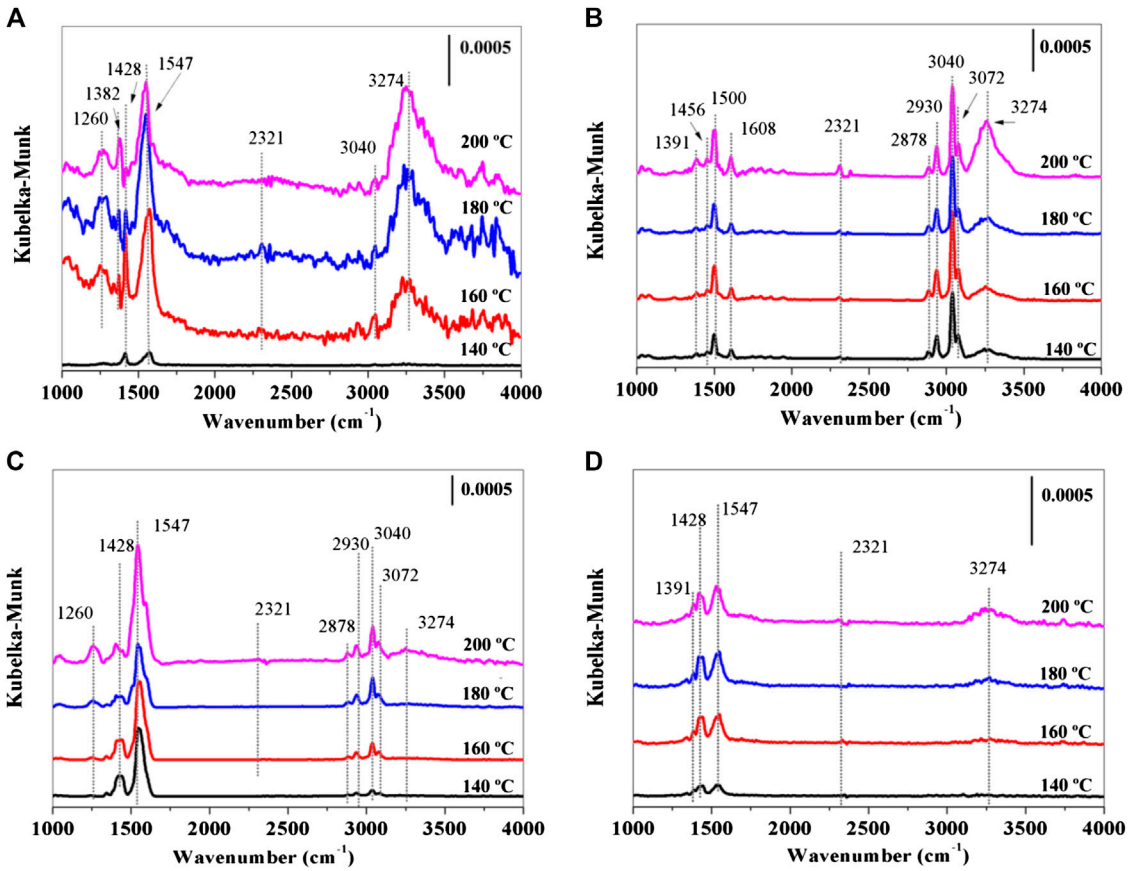

FIGURE 9 | *In situ* DRIFTS of toluene oxidation over **(A)** OL, **(B)** OMS, **(C)** CeOL, and **(D)** CeOMS catalysts.

CONCLUSIONS

In summary, OMS-2, OL-1, Ce/OMS-2 and Ce/OL-1 materials were prepared and adopted for catalytic oxidation of toluene. We found that OMS-2 presents excellent activity achieving 90% of toluene (1,000 ppm) oxidized at 224°C. Both the crystal planes of OMS-2 and OL-1 material are the (200) D-space of MnO_2. After addition of Ce, the lattice planes change to (110) and (310) for Ce/OL-1 Ce/OMS-2 materials, respectively. However, the crystal phase of prepared materials is not the main factor influencing catalytic performance in toluene oxidation. Ce ions occupy a certain amount of active sites and block the toluene oxidation process over prepared manganese oxides. With less amounts of lattice oxygen and lower reducibility, the Ce-containing catalysts lead to a decrease in catalytic activity. Besides, the introduction of Ce can prolong the reaction time and produce more byproducts by raising the amounts of acid sites.

DATA AVAILABILITY STATEMENT

All datasets presented in this study are included in the article.

AUTHOR CONTRIBUTIONS

All authors listed have made a substantial, direct, and intellectual contribution to the work and approved it for publication.

FUNDING

This work was supported by the National Natural Science Foundation of China (21876139, 21922606, 21577046), the Key R&D Program of Shaanxi Province (2019SF-244, 2019ZDLSF05-05-02), the Hubei Provincial Natural Science Foundation of China (2019CFB578), and the Hubei Province Technical Innovation Special Major Project (2019ACA160).

ACKNOWLEDGMENTS

The authors gratefully acknowledge the supports of K. C. Wong Education Foundation and instrumental analysis center of Xi'an Jiaotong University as well as the editor and reviewers for their professional work and valuable comments.

REFERENCES

Arena, F., Gumina, B., Lombardo, A. F., Espro, C., Patti, A., Spadaro, L., et al. (2015). Nanostructured MnO_x catalysts in the liquid phase selective oxidation of benzyl alcohol with oxygen: part I. Effects of Ce and Fe addition on structure and reactivity. *Appl. Catal. B Environ.* 162, 260–267. doi:10.1016/j.apcatb.2014.06.054

Arzamendi, G., Delapenaoshea, V., Alvarezgalvan, M., Fierro, J., Arias, P., and Gandia, L. (2009). Kinetics and selectivity of methyl-ethyl-ketone combustion in air over alumina-supported PdOx-MnOx catalysts. *J. Catal.* 261, 50–59. doi:10.1016/j.jcat.2008.11.001

Chen, J., Chen, X., Chen, X., Xu, W., Xu, Z., Jia, H., et al. (2018). Homogeneous introduction of CeOy into MnOx-based catalyst for oxidation of aromatic VOCs. *Appl. Catal. B Environ.* 224, 825–835. doi:10.1016/j.apcatb.2017.11.036

Chen, X., Chen, X., Yu, E., Cai, S., Jia, H., Chen, J., et al. (2018). *In situ* pyrolysis of Ce-MOF to prepare CeO_2 catalyst with obviously improved catalytic performance for toluene combustion. *Chem. Eng. J.* 344, 469–479. doi:10.1016/j.cej.2018.03.091

Chen, Y., Zheng, H., Guo, Z., Zhou, C., Wang, C., Borgna, A., et al. (2011). Pd catalysts supported on MnCeOx mixed oxides and their catalytic application in solvent-free aerobic oxidation of benzyl alcohol: support composition and structure sensitivity. *J. Catal.* 283, 34–44. doi:10.1016/j.jcat.2011.06.021

He, C., Cheng, J., Zhang, X., Douthwaite, M., Pattisson, S., and Hao, Z. (2019). Recent advances in the catalytic oxidation of volatile organic compounds: a review based on pollutant sorts and sources. *Chem. Rev.* 119, 4471–4568. doi:10.1021/acs.chemrev.8b00408

He, C., Li, P., Cheng, J., Wang, H., Li, J., Li, Q., et al. (2010). Synthesis and characterization of Pd/ZSM-5/MCM-48 biporous catalysts with superior activity for benzene oxidation. *Appl. Catal. Gen.* 382, 167–175. doi:10.1016/j.apcata.2010.04.033

Hou, J., Li, Y., Mao, M., Ren, L., and Zhao, X. (2014). Tremendous effect of the morphology of birnessite-type manganese oxide nanostructures on catalytic activity. *ACS Appl. Mater. Interfaces.* 6, 14981–14987. doi:10.1021/am5027743

Iyer, A., Del-Pilar, J., King'ondu, C. K., Kissel, E., Garces, H. F., Huang, H., et al. (2012). Water oxidation catalysis using amorphous manganese oxides, octahedral molecular sieves (OMS-2), and octahedral layered (OL-1) manganese oxide structures. *J. Phys. Chem. C* 116, 6474–6483. doi:10.1021/jp2120737

Jiang, Z., He, C., Dummer, N. F., Shi, J., Tian, M., Ma, C., et al. (2018). Insight into the efficient oxidation of methyl-ethyl-ketone over hierarchically micro-mesostructured Pt/K-(Al)SiO_2 nanorod catalysts: structure-activity relationships and mechanism. *Appl. Catal. B Environ.* 226, 220–233. doi:10.1016/j.apcatb.2017.12.007

Kingondu, C. K., Opembe, N., Chen, C. H., Ngala, K., Huang, H., Iyer, A., et al. (2011). Manganese oxide octahedral molecular sieves (OMS-2) multiple framework substitutions: a new route to OMS-2 particle size and morphology control. *Adv. Funct. Mater.* 21, 312–323. doi:10.1002/adfm.201001020

Li, J., Wang, R., and Hao, J. (2010). Role of lattice oxygen and lewis acid on ethanol oxidation over OMS-2 catalyst. *J. Phys. Chem. C* 114, 10544–10550. doi:10.1021/jp102779u

Li, X., Zhu, Z., Zhao, Q., and Wang, L. (2011). Photocatalytic degradation of gaseous toluene over $ZnAl_2O_4$ prepared by different methods: a comparative study. *J. Hazard Mater.* 186, 2089–2096. doi:10.1016/j.jhazmat.2010.12.111

Liu, X.-S., Jin, Z.-N., Lu, J.-Q., Wang, X.-X., and Luo, M.-F. (2010). Highly active CuO/OMS-2 catalysts for low-temperature CO oxidation. *Chem. Eng. J.* 162, 151–157. doi:10.1016/j.cej.2010.05.015

Luo, J., Zhang, Q., Huang, A., and Suib, S. L. (2000). Total oxidation of volatile organic compounds with hydrophobic cryptomelane-type octahedral molecular sieves. *Microporous Mesoporous Mater.* 35–36, 209–217. doi:10.1016/S1387-1811(99)00221-8

Luo, M.-F., Hou, Z.-Y., Yuan, X.-X., and Zheng, X.-M. (1998). Characterization study of CeO_2 supported Pd catalyst for low-temperature carbon monoxide oxidation. *Catal. Lett.* 50, 205–209. doi:10.1023/A:1019023220271

Luo, S., Duan, L., Sun, B., Wei, M., Li, X., and Xu, A. (2015). Manganese oxide octahedral molecular sieve (OMS-2) as an effective catalyst for degradation of organic dyes in aqueous solutions in the presence of peroxymonosulfate. *Appl. Catal. B Environ.* 164, 92–99. doi:10.1016/j.apcatb.2014.09.008

Menon, U., Galvita, V. V., and Marin, G. B. (2011). Reaction network for the total oxidation of toluene over CuO-CeO_2/Al_2O_3. *J. Catal.* 283, 1–9. doi:10.1016/j.jcat.2011.05.024

Monney, L., Belali, R., Vebrel, J., Dubois, C., and Chambaudet, A. (1998). Photochemical degradation study of an epoxy material by IR-ATR spectroscopy. *Polym. Degrad. Stabil.* 62, 353–359. doi:10.1016/S0141-3910(98)00018-4

Nyutu, E. K., Chen, C.-H., Sithambaram, S., Crisostomo, V. M. B., and Suib, S. L. (2008). Systematic control of particle size in rapid open-vessel microwave synthesis of K-OMS-2 nanofibers. *J. Phys. Chem. C* 112, 6786–6793. doi:10.1021/jp800672m

Pan, H., Jian, Y., Chen, C., He, C., Hao, Z., Shen, Z., et al. (2017). Sphere-shaped Mn_3O_4 catalyst with remarkable low-temperature activity for methyl-ethyl-ketone combustion. *Environ. Sci. Technol.* 51, 6288–6297. doi:10.1021/acs.est.7b00136

Qu, Z., Bu, Y., Qin, Y., Wang, Y., and Fu, Q. (2013). The improved reactivity of manganese catalysts by Ag in catalytic oxidation of toluene. *Appl. Catal. B Environ.* 132–133, 353–362. doi:10.1016/j.apcatb.2012.12.008

Santos, V. P., Carabineiro, S. A. C., Bakker, J. J. W., Soares, O. S. G. P., Chen, X., Pereira, M. F. R., et al. (2014). Stabilized gold on cerium-modified cryptomelane: highly active in low-temperature CO oxidation. *J. Catal.* 309, 58–65. doi:10.1016/j.jcat.2013.08.030

Shen, Y.-F., Suib, S. L., and O'Young, C.-L. (1996). Cu containing octahedral molecular sieves and octahedral layered materials. *J. Catal.* 161, 115–122. doi:10.1006/jcat.1996.0168

Sun, H., Chen, S., Wang, P., and Quan, X. (2011). Catalytic oxidation of toluene over manganese oxide octahedral molecular sieves (OMS-2) synthesized by different methods. *Chem. Eng. J.* 178, 191–196. doi:10.1016/j.cej.2011.10.047

Sun, M., Yu, L., Ye, F., Diao, G., Yu, Q., Hao, Z., et al. (2013). Transition metal doped cryptomelane-type manganese oxide for low-temperature catalytic combustion of dimethyl ether. *Chem. Eng. J.* 220, 320–327. doi:10.1016/j.cej.2013.01.061

Tang, W., Wu, X., Liu, G., Li, S., Li, D., Li, W., et al. (2015). Preparation of hierarchical layer-stacking Mn-Ce composite oxide for catalytic total oxidation of VOCs. *J. Rare Earths.* 33, 62–69. doi:10.1016/S1002-0721(14)60384-7

Tian, H., He, J., Zhang, X., Zhou, L., and Wang, D. (2011). Facile synthesis of porous manganese oxide K-OMS-2 materials and their catalytic activity for formaldehyde oxidation. *Microporous Mesoporous Mater.* 138, 118–122. doi:10.1016/j.micromeso.2010.09.022

Tian, M., He, C., Yu, Y., Pan, H., Smith, L., Jiang, Z., et al. (2018). Catalytic oxidation of 1,2-dichloroethane over three-dimensional ordered meso-macroporous Co_3O_4/$La_{0.7}Sr_{0.3}Fe_{0.5}Co_{0.5}O_3$: destruction route and mechanism. *Appl. Catal. A Gen.* 553, 1–14. doi:10.1016/j.apcata.2018.01.013

Wang, R., and Li, J. (2010). Effects of precursor and sulfation on OMS-2 catalyst for oxidation of ethanol and acetaldehyde at low temperatures. *Environ. Sci. Technol.* 44, 4282–4287. doi:10.1021/es100253c

Wang, R., and Li, J. (2009). OMS-2 catalysts for formaldehyde oxidation: effects of Ce and Pt on structure and performance of the catalysts. *Catal. Lett.* 131, 500–505. doi:10.1007/s10562-009-9939-5

Wang, Y., Deng, W., Wang, Y., Guo, L., and Ishihara, T. (2018). A comparative study of the catalytic oxidation of chlorobenzene and toluene over Ce-Mn oxides. *Mol. Catal.* 459, 61–70. doi:10.1016/j.mcat.2018.08.022

Wu, J., Xia, Q., Wang, H., and Li, Z. (2014). Catalytic performance of plasma catalysis system with nickel oxide catalysts on different supports for toluene removal: effect of water vapor. *Appl. Catal. B Environ.* 156-157, 265–272. doi:10.1016/j.apcatb.2014.03.017

Wu, Z., Deng, J., Xie, S., Yang, H., Zhao, X., Zhang, K., et al. (2016). Mesoporous Cr2O3-supported Au-Pd nanoparticles: high-performance catalysts for the oxidation of toluene. *Microporous Mesoporous Mater.* 224, 311–322. doi:10.1016/j.micromeso.2015.11.061

Yan, Z., Xu, Z., Yang, Z., Yue, L., and Huang, L. (2019). Graphene oxide/Fe2O3 nanoplates supported Pt for enhanced room-temperature oxidation of formaldehyde. *Appl. Surf. Sci.* 467–468, 277–285. doi:10.1016/j.apsusc.2018.10.123

Yu, L., Diao, G., Ye, F., Sun, M., Zhou, J., Li, Y., et al. (2011). Promoting effect of Ce in Ce/OMS-2 catalyst for catalytic combustion of dimethyl ether. *Catal. Lett.* 141, 111–119. doi:10.1016/j.jcat.2013.08.030

Zhang, J., Zhang, J. H., Zhang, C. B., and He, H. (2015). Complete catalytic oxidation of ethanol over MnO_2 with different crystal phase structures. *Acta Phys. Chim. Sin.* 31, 353–359. doi:10.3866/PKU.WHXB201412081

Zhang, L., Tu, J., Lyu, L., and Hu, C. (2016). Enhanced catalytic degradation of ciprofloxacin over Ce-doped OMS-2 microspheres. *Appl. Catal. B Environ.* 181, 561–569. doi:10.1016/j.apcatb.2015.08.029

Zhou, J., Zhao, L., Huang, Q., Zhou, R., and Li, X. (2009). Catalytic activity of Y zeolite supported CeO_2 catalysts for deep oxidation of 1, 2-dichloroethane (DCE). *Catal. Lett.* 127, 277–284. doi:10.1007/s10562-008-9672-5

Zhu, Z., Liu, F., and Zhang, W. (2015). Fabricate and characterization of Ag/$BaAl_2O_4$ and its photocatalytic performance towards oxidation of gaseous toluene studied by FTIR spectroscopy. *Mater. Res. Bull.* 64, 68–75. doi:10.1016/j.materresbull.2014.12.026

Conflict of Interest: The authors declare that the research was conducted in the absence of any commercial or financial relationships that could be construed as a potential conflict of interest.

Copyright © 2020 Yue, Hu, Tian, Liao, Xu, Shi and He. This is an open-access article distributed under the terms of the Creative Commons Attribution License (CC BY). The use, distribution or reproduction in other forums is permitted, provided the original author(s) and the copyright owner(s) are credited and that the original publication in this journal is cited, in accordance with accepted academic practice. No use, distribution or reproduction is permitted which does not comply with these terms.